Research Article | Vol. 13, No. 7 / 1 Jul 2022 / Biomedical Optics Express 4047

Biomedical Optics EXPRESS

# High-resolution sub-millimetre diameter side-viewing all-optical ultrasound transducer based on a single dual-clad optical fibre

RICHARD J. COLCHESTER,[1,2,*] EDWARD Z. ZHANG,[1,2] PAUL C. BEARD,[1,2] AND ADRIEN E. DESJARDINS[1,2]

[1] *Department of Medical Physics and Biomedical Engineering, University College London, Gower Street, London, WC1E 6BT, UK*

[2] *Wellcome/EPSRC Centre for Interventional and Surgical Sciences, 43-45 Foley Street, London, W1W 7TY, UK*

[*] *richard.colchester@ucl.ac.uk*

**Abstract:** All-optical ultrasound (OpUS), where ultrasound is both generated and received using light, has emerged as a modality well-suited to highly miniaturised applications. In this work we present a proof-of-concept OpUS transducer built onto a single optical fibre with a highly miniaturised lateral dimension (<0.8 mm). A key innovation was to use a dual-clad optical fibre (DCF) to provide multimode light for ultrasound generation and single mode light for ultrasound reception. The transducer comprised a proximal section of DCF spliced to a short section of single mode fibre (SMF). Multimode light was outcoupled at the splice joint and guided within a square capillary to provide excitation for ultrasound generation. Whilst single mode light was guided to the distal tip of the SMF to a plano-concave microresonator for ultrasound reception. The device was capable of generating ultrasound with pressures >0.4 MPa and a corresponding bandwidth >27 MHz. Concurrent ultrasound generation and reception from the transducer enabled imaging via motorised pull-back allowing image acquisition times of 4 s for an aperture of 20 mm. Image resolution was as low as ~50 μm and 190 μm in the axial and lateral extents, respectively, without the need for image reconstruction. Porcine aorta was imaged *ex vivo* demonstrating detailed ultrasound images. The unprecedented level of miniaturisation along with the high image quality produced by this device represents a radical new paradigm for minimally invasive imaging.



## 1. Introduction

Minimally invasive surgery has been replacing open surgery due to its benefits in terms of reduced recovery time, scarring and discomfort. However, without direct line of sight surgeons must rely on imaging technologies for guidance and diagnosis. Recent years have seen the development of several technologies to provide this, including miniaturised ultrasound devices [1–3] and optical coherence tomography [4,5]. Whilst these technologies can provide detailed images, they each have limitations, including device cost, resolution, imaging depth and miniaturisation.

All-optical ultrasound is emerging as an alternative imaging paradigm that is well-suited to these highly miniaturised applications. Here, ultrasound is both generated and received optically, enabling device miniaturisation through the use of optical fibres. For ultrasound generation pulsed or modulated laser light is absorbed within a coating material leading to a transient increase in temperature [6]. The corresponding pressure rise then propagates as ultrasound. Recent years have seen the development of several novel materials for ultrasound generation [7–16], leading to improved efficiencies and even the ability to include complementary modalities [8,10]. For ultrasound reception interferometric methods have been used [17], including resonators such as microring resonators [18,19], Fibre Bragg gratings [20,21] and Fabry-Pérot cavities [22–25].

#459486 https://doi.org/10.1364/BOE.459486
Journal © 2022 Received 24 Mar 2022; revised 13 May 2022; accepted 13 May 2022; published 27 Jun 2022

Biomedical Optics EXPRESS

Through the use of optical fibres, these transmit and receive elements can be paired to create a miniature ultrasound transducer.

Thus far separate optical fibres have been used for ultrasound generation and reception [8,26–30]. Such devices have been demonstrated in a forward-viewing format for synthetic aperture imaging on the bench top [8,10,26,29,30] and M-mode imaging of both a dynamic phantom [31] and *in vivo* [28]. However, a side-viewing setup, which enables ultrasound generation and reception perpendicular to the longitudinal axis of the optical fibre is preferential for many surgical scenarios, such as intravascular imaging. This has been demonstrated on the bench top using a modified optical fibre tip to redirect the light from the optical fibre to a side surface for ultrasound transmission [27]. By rotating only the transmitting fibre, rotational imaging in an *ex vivo* swine carotid artery was demonstrated [27]. However, using two optical fibres limits the miniaturisation of the device and increases the complexity of integration into a medical catheter. Combining transmit and receive elements of the optical transducer could allow for a further level of miniaturisation and a reduction in device complexity to be realised.

Previously, a device using a single mode optical fibre (SMF) in a forward-viewing format has been proposed [32]. However, this work has yet to demonstrate concurrent ultrasound generation and reception or imaging. Further, the use of SMF for ultrasound generation limits the optical power that can be delivered to the coating for excitation. In this work, we overcome these limitations by using a dual-clad optical fibre (DCF) for light delivery. Additionally, we used micro-optic components to enable ultrasound transmission in a side-viewing fashion which is of higher clinical interest. The OpUS transducer was employed for imaging and demonstrated high-resolution images with acquisition times of 4 s. These innovations represent a radical step forward for the OpUS technology platform that could extend its applications in minimally invasive procedures.

## 2. Methods

### 2.1. Transducer design and fabrication

This work presents a design for fabricating a side-viewing OpUS transducer on a single optical fibre. To achieve this two central challenges were addressed: combining both multimode light delivery for ultrasound generation and single mode light delivery for ultrasound reception into a single optical fibre, and guiding excitation light for ultrasound generation to a side facing optically absorbing coating (Fig. 1).

Optical ultrasound generation and reception require the use of different optical fibres. Generation of significant ultrasound pressures (>0.1 MPa) requires multimode optical fibres to deliver sufficient optical fluence to the ultrasound generating surfaces. Conversely, reception of ultrasound requires single mode optical fibres for the delivery of interrogation light to the highly sensitive plano-concave microresonators. Typically, two separate optical fibres are used to provide these different optical channels [26,28]. To overcome this, we employed a dual-clad optical fibre, which had a core, inner cladding, and outer cladding. Single-mode light for ultrasound reception was guided within the fibre core, whilst multimode light for ultrasound generation was guided within the inner cladding by the outer cladding.

The fabrication process followed several steps outlined in Fig. 1(a). Firstly, a 2 m length of DCF (core diameter: 9 µm, inner cladding diameter: 105 µm, outer cladding diameter: 125 µm, DCF13, Thorlabs, UK) and a 8 cm length of SMF (cladding diameter: 80 µm, SM1250G80, Thorlabs, UK) were prepared for splicing. These fibres were chosen due to the well-matched mode field diameter of the single mode core, as well as the step-down in cladding diameter (125 to 80 µm). This step-down in cladding diameter from the DCF to the SMF provided a discontinuity to improve the extraction of multimode light for ultrasound generation at the splice point. The fibres were spliced using an automated splicer (FSM-70S+, Fujikura Europe Ltd, UK) and manufacturer-provided settings for splicing dissimilar cladding diameter single mode fibres.

Biomedical Optics EXPRESS

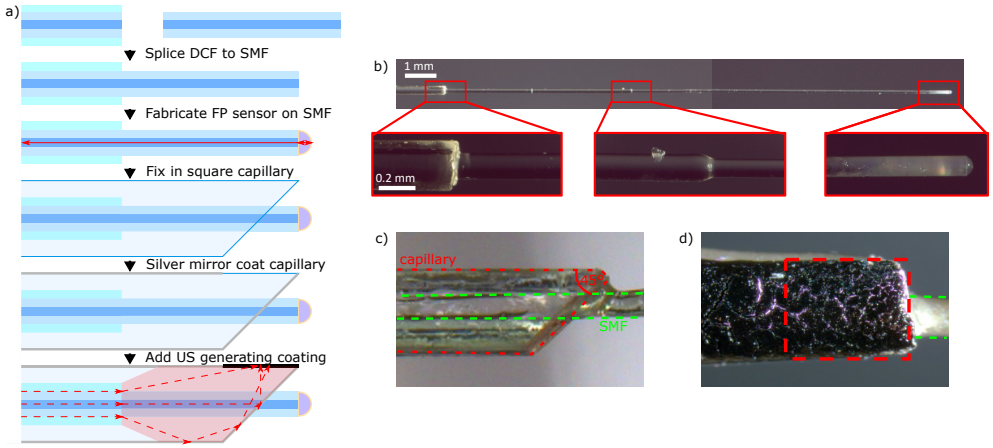


**Fig. 1.** a) Schematic of the OpUS transducer fabrication process. b) Microscope images of the OpUS transducer prior to adding the square glass capillary, with magnifications showing: the optical fibre buffer coating (left), the splice joint (middle), and the plano-concave microresonator (right). c) Side on microscope image of the spliced optical fibres (green dashed region) after adding the 45° polished square glass capillary (red dashed region) d) Front on microscope image of the ultrasound generating surface (red dashed region) on the OpUS transducer.

After splicing, the SMF was cleaved at a distance of 1 cm from the splice point, leaving a 2 m length of DCF spliced to a 1 cm length of SMF (Fig. 1(a), (b)).

Following splicing, a plano-concave microresonator was constructed on the distal end of the SMF using a method which has been previously described [22,23]. Briefly, a dielectric mirror coating was applied to the cleaved fibre end surface. Subsequently, an epoxy dome was added using a dip coating method. Finally, a second dielectric coating was applied to the outer surface of the epoxy dome (Fig. 1(b)). The dielectric coatings had a nominal reflectivity of 98%.

Subsequently, the ultrasound transmitter was fabricated on the fibre. To generate ultrasound laterally from the optical fibre, the structure had to be modified. For this, a square glass capillary (ID: 0.3 × 0.3 mm, wall thickness: 0.15 mm, 8330-100, CM Scientific Ltd, UK) was used. This was chosen to guide and collect extracted multimode light at the splice joint and to provide a planar surface for ultrasound generation. Firstly, the square glass capillary was manually cleaved to a length of 2 cm using a tungsten blade. Following this, the distal end of the capillary was polished to 45°. The 45° end was designed to redirect multimode light to the capillary side surface where ultrasound generation could occur. The prepared optical fibre with the plano-concave microresonator on its distal end was inserted through the capillary from the unpolished end, such that the plano-concave microresonator extended out of the capillary at the end with the 45° polished surface (Fig. 1(a), (c)) and the distal tip of the fibre extended *ca.* 0.2 mm out of the capillary. Subsequently, the capillary was fixed in place using a UV curable epoxy (NOA61, Norland Optics, USA) by filling the capillary until the epoxy formed a flat meniscus at the distal end and curing with a UV LED.

Following the attachment of the capillary to the optical fibre assembly, the capillary was coated with a silver mirror paint (123-9911, RS Components Ltd, UK). The paint was applied manually with a small brush and a small window (*ca.* 0.55 × 0.55 mm) was left uncoated opposite the 45° polished surface, for excitation light to escape for ultrasound generation (Fig. 1(a)). Subsequently, a composite comprising reduced graphene oxide (rGO) and polydimethylsiloxane (PDMS) was applied to the capillary over the window. The composite was made using a protocol previously

Biomedical Optics EXPRESS

described [9]. Briefly, rGO (805084, Sigma Aldrich, UK) was mixed with xylene to create a homogeneous solution. This solution was applied to the capillary surface by contacting the surface with a droplet of rGO solution on a small brush. The coating was allowed to dry and was subsequently overcoated with a droplet of PDMS (MED-1000, Polymer Systems Technology, UK) which had been thinned with xylene. The coating was left to cure in ambient conditions for 24 hours.

### 2.2. Console design

For operation the OpUS transducer was connected to a console for ultrasound generation and reception (Fig. 2). For ultrasound generation pulsed light was delivered into the OpUS transducer from a Q-switched Nd:YAG laser (SPOT-10-500-1064, Elforlight, UK) via a dual-clad fibre coupler (DC1300LQ1, Thorlabs, UK). The fibre coupler had a coupling efficiency of >75% at 1064 nm. The laser had a wavelength of 1064 nm, a pulse width of 2 ns and a pulse energy of 40 µJ. For ultrasound reception, continuous-wave light was delivered into the ultrasound receiving fibre from a tuneable laser (Tunics T100S-HP CL, Yenista Optics, France), via a circulator and the dual-clad fibre coupler. This laser had a wavelength range of 1500 – 1600 nm and an output power level of 6 mW. The reflected optical signal was received using a custom 50 MHz photodiode-transimpedance amplifier unit which split the signal into low (<50 kHz) and high (>500 kHz) frequency components [26]. The low frequency component was digitised at 16 bits with a sample rate of 1 MS/s and used to acquire the interferometer transfer function (ITF) of the sensor and identify the optimum bias wavelength. The high frequency component was digitised at 14 bits with a sample rate of 100 MS/s and was encoded with the received ultrasound signals. For image acquisition, the OpUS transducer was connected to a motorised translation stage (MTS50/M-Z8, Thorlabs, Germany) and translated at a constant rate.

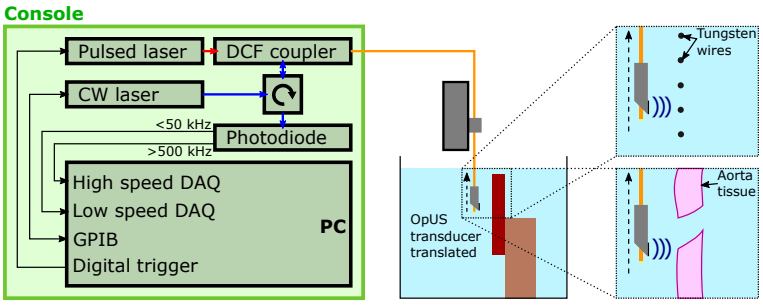


**Fig. 2.** Schematic of the experimental setup used for OpUS imaging with the single fibre OpUS transducer. Console with the pulsed laser for ultrasound excitation, CW laser for ultrasound reception, circulator, dual clad fibre (DCF) coupler, photodiode and PC for control shown (left). Imaging schematic showing OpUS transducer translation via a motorised stage and imaging target (red box) with close up schematics of the imaging targets used: a tungsten wire phantom and *ex vivo* aorta imaging setups (right).

### 2.3. Transducer characterisation

The performance of the OpUS transducer was characterised prior to use for imaging. To assess the efficacy of the light extraction, the proportion of light redirected by the silver mirror through the optical window was compared to the total light emitted from the distal section of the transducer, including the full capillary length and the plano-concave microresonator, prior to coating with the ultrasound generating composite. The optical window was the region on the transducer left clear of silver mirror where the ultrasound generating coating was subsequently applied. To evaluate

Biomedical Optics EXPRESS

this the uncoated transducer was coupled to a broadband halogen lamp (HL-2000-HP-FHSA, Ocean Optics, USA) via the dual-clad fibre coupler. An integrating sphere was used to collect light from the OpUS transducer and the output of the integrating sphere was coupled to a spectrometer. Two measurements were taken. Firstly with the OpUS transducer outside the integrating sphere with the optical window on the OpUS transducer facing into the entry port to the integrating sphere. This was to measure the light redirected by the mirror for ultrasound generation. Secondly, the OpUS transducer was inserted into the integrating sphere and the total light from the device was measured. The proportion of light redirected was calculated by comparing the two measurements.

The ITF of the plano-concave microresonator was measured using the console designed for image acquisition. A wavelength sweep was carried out from 1520 to 1570 nm at an optical power of 0.5 mW. The reflected optical power at each wavelength was recorded using a custom photoreceiver. These plano-concave microresonators have previously been demonstrated to have a highly omnidirectional sensitivity and a noise equivalent pressure of <100 Pa.

The transmitted ultrasound was characterised using a 200 μm diameter needle hydrophone (Precision Acoustics Ltd, UK) with a calibrated range of 1 – 30 MHz. An ultrasound field scan was performed by scanning the hydrophone over a two dimensional grid orthogonal to the transmitted ultrasound beam direction. The grid measured 3 mm × 3 mm with an isotropic step size of 50 μm and was positioned at an axial distance of 1.5 mm from the ultrasound generating coating on the surface of the OpUS transducer.

### 2.4. Tungsten wire and ex vivo imaging

For OpUS imaging the transducer was mounted on a motorized translation stage (MTS50/M-Z8, Thorlabs, Germany). For all images acquired the transducer was translated at a constant velocity of 5 mm/s over a linear distance of 20 mm resulting in an image acquisition time of 4 s. For imaging, A-lines were acquired at a rate of 200 Hz, corresponding to an A-line separation of 25 μm. The acquired ultrasound A-lines were processed and formed into an image following several steps. A-lines where concatenated in time and the data was bandpass filtered (Butterworth, $4^{th}$ order, 2.5 – 45 MHz), followed by cross-talk removal to remove signal transmitted directly from the transmitter to the receiver. This cross-talk algorithm has been previously described [26]. Briefly, each scan was fitted with a general linear model to model the cross-talk. The modelled cross-talk was then subtracted from the filtered A-line. Subsequently, a two-dimensional Wiener filter was applied to the data, followed by median filtering to reduce the background noise. Finally, a Hilbert transform was applied to extract the signal envelope and the data was log transformed for display.

To assess the imaging resolution of the OpUS transducer, a tungsten wire phantom was used. The phantom comprised a series of tungsten wires (diameter: 27 μm) spaced at regular intervals on a plastic frame. The device was translated such that device motion was perpendicular to the longitudinal axis of the tungsten wires, with the ultrasound generating surface facing the wires (Fig. 2). A total of 5 images was acquired with the phantom at increasing depths to assess the relationship between image resolution and depth. To obtain the axial and lateral resolutions from the resulting image, cross-sections were taken through the resultant point-spread-functions in the image. The full-width half-maximum (−6 dB level) of these was taken as the imaging resolution.

To demonstrate tissue imaging a section of porcine aorta was used. The porcine aorta section was cut along its longitudinal axis to allow it to be fixed to a mount for imaging. Imaging was carried out over a region containing a side branch and the device was translated such that device motion was parallel to the longitudinal vessel axis, mimicking a pull-back within the vessel (Fig. 2).

Biomedical Optics EXPRESS

## 3. Results

### 3.1. Transducer characteristics

Visual inspection of the devices with a stereo-microscope showed a uniform coating of the silver mirror over the capillary and a clear window prior to coating with the rGO-PDMS composite. The rGO-PDMS composite coating demonstrated an even conformal coating over the capillary surface. The efficacy of light extraction and redirection to ultrasound generating coating was compared to the total light exiting the distal end of the optical fibre. It was found that *ca.* 52% of the light was redirected to the optical window where the ultrasound generating composite was coated. The remaining light escaped from other surfaces at the distal section of the transducer, including the distal tip. The ITF was measured prior to use for imaging and was similar to those previously reported [23] (Fig. 3(a)). The ITF demonstrated a free spectral range of 26.9 nm and a visibility of 0.88.

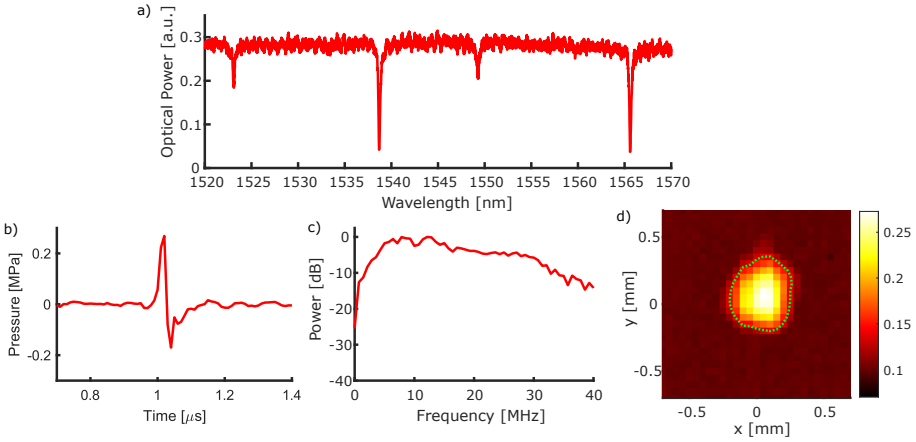


**Fig. 3.** a) Measured interferometer transfer function of the plano-concave microresonator ultrasound receiver. b) Generated ultrasound time-series as measured at 1.5 mm from the ultrasound generating coating. c) Corresponding generated ultrasound bandwidth. d) Generated ultrasound beam profile as measured at 1.5 mm from the ultrasound generating coating with a green contour line showing the full-width at half maximum (scale in MPa).

The generated ultrasound was characterised prior to use for imaging. The generated peak-to-peak ultrasound pressure as measured at 1.5 mm from the coating surface was 0.44 MPa (Fig. 3(b)). The ultrasound pulse was bipolar in shape, typical of previously reported optical ultrasound transmitters [26,27]. The corresponding −6 dB ultrasound bandwidth was 27.1 MHz, with a centre frequency of *ca.* 15 MHz (Fig. 3(c)). The generated ultrasound beam profile at 1.5 mm was approximately circular with a full-width half-maximum beam width of *ca.* 0.5 mm (Fig. 3(d)).

### 3.2. Tungsten wire and ex vivo imaging

The tungsten wires on the resolution phantom appeared in the OpUS images as elliptical points (Fig. 4(a)). To find the axial and lateral resolution a cross-section was taken in the depth and $x$ dimensions, respectively, for each point appearing in the image (Fig. 4(b)). Both the axial and lateral resolution remained stable with increasing depth from 1.5 to 3.5 mm (Fig. 4(c)). The axial resolution was better than the lateral resolution, with a value of 97 ± 26 μm. The lateral resolution had an average value of 267 ± 49 μm. The minimum values for the axial and lateral resolutions were 52 μm and 184 μm, respectively.

Biomedical Optics EXPRESS

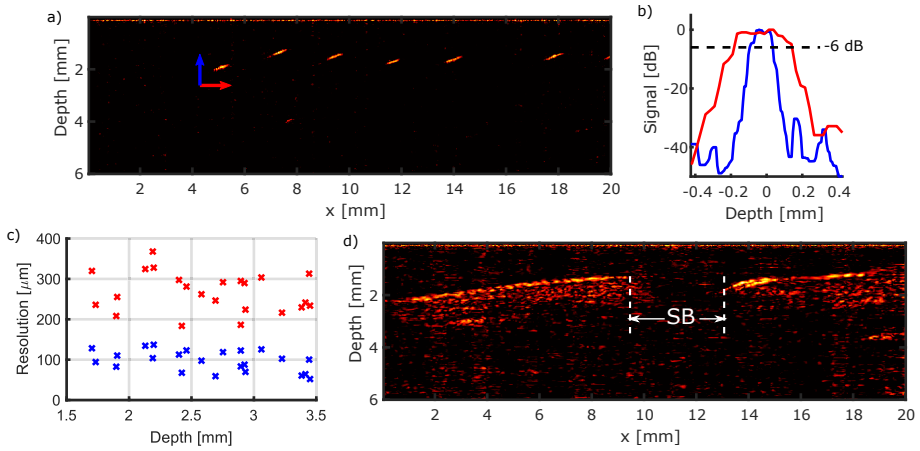


**Fig. 4.** a) Example OpUS image of a tungsten wire resolution phantom, with arrows to show the direction of cross-sections used to calculate the axial (blue arrow) and lateral (red arrow) resolutions. b) Example cross-sections through a point-spread-function as used to calculate the axial (blue line) and lateral (red line) resolution (log scale). c) Axial (blue crosses) and lateral (red crosses) resolution of the OpUS device found from the acquired OpUS images. d) OpUS image of an *ex vivo* porcine aorta with side branch (SB: located at *ca.* x = 10 – 13 mm).

Porcine vascular tissue was imaged to demonstrate the capability of the OpUS transducer for tissue imaging. The porcine aorta was easily distinguished in the image against the background noise (SNR: 26 dB) (Fig. 4(d)). The inner surface of the aorta (closest to the transducer) was visible as a bright surface, with a higher signal than the underlying tissue. The subsurface vessel wall was presented as a speckled region around 1 – 2 mm in thickness. The side branch in the aorta was well defined as a region with no signal, presented as a gap in the vessel at *ca.* 10 – 13 mm in Fig. 4(d).

## 4. Discussion & conclusion

In this study, we present a novel side-viewing ultrasound transducer that was fabricated on a single optical fibre. Several advances were made over previous studies, including device miniaturisation (<1 mm lateral width), combining the transmit and receive elements on a single optical fibre, greatly reduced image acquisition time for linear imaging (from >1 minute [26] to 4 s), and high imaging resolution without the need for image reconstruction. These advances represent crucial steps towards moving this technology to the clinic.

The OpUS transducer demonstrated here was fabricated on a dual-clad optical fibre, thereby allowing the delivery of multimode light for ultrasound excitation and single mode light for ultrasound reception. The use of a square glass capillary to guide extracted excitation light from the optical fibre provided a planar surface for ultrasound generation and allowed the fabrication of a device with sub-millimetre lateral dimensions. This unprecedented level of miniaturisation is promising for opening new minimally invasive imaging applications, where minimising device lateral dimensions is crucial. Further, fabricating the device on a single fibre with co-linear light delivery will allow for simpler integration into catheters and devices for application to surgery.

The light extraction and generated ultrasound were characterised. It was found that *ca.* 50% of the light delivered for ultrasound excitation was directed to the ultrasound generating surface. The light which escaped was found to have no effect on the plano-concave microresonator stability and did not generate a photoacoustic signal during imaging. The light extraction could be optimised

Biomedical Optics EXPRESS

in future devices by adjusting the capillary length to balance light extraction with losses from scattering and absorption within the structure. Further, in this work, a simple silver paint was used to provide a reflective surface, the efficiency of this mirror might be improved by using dielectric coatings or sputtered mirror coatings, at the cost of increased manufacturing complexity and cost. Additionally, this device relied on the meniscus of the epoxy filling at the 45° polished end of the capillary to provide a surface for reflecting light towards the ultrasound generating surface. As an alternative, future devices could comprise custom 3D printed glass or polymer structures [33–35] as opposed to a square capillary to provide this surface.

The plano-concave microresonator demonstrated a high fringe visibility and steep ITFs, in-line with previously fabricated and presented hydrophone devices [22,24]. The generated ultrasound beam was characterised with a calibrated needle hydrophone and the measured peak-to-peak ultrasound pressure exceeded 0.4 MPa at a distance of 1.5 mm. Whilst this was lower than some previously reported optical ultrasound generators [8–10], it was still sufficient for tissue imaging without the need for averaging. Further, due to losses in coupling from the excitation laser the excitation laser pulse energy was comparably lower than in previous studies. This could be improved in future studies with the use of a higher pulse energy laser and matching between the laser output fibre diameter and DCF coupler. It is expected that an increase in this laser energy would lead to a proportional increase in generated ultrasound pressure as with previous studies [7,10]. This should be possible as the fluence used was lower than that used in previous OpUS devices with similar coatings [9], suggesting it was below the damage threshold. The corresponding ultrasound bandwidth was 27.1 MHz, which is comparable to previous high-bandwidth OpUS transducers used for *ex vivo* and *in vivo* imaging [8,26,28].

In this work, a constant linear pull-back was used for image acquisition, providing high resolution images. The use of a constant pull-back resulted in acquisition times much shorter than those previously reported which used a raster scanning approach with the probe pausing at each location for data acquisition [26,29,30]. The pull-back velocity used was limited to 5 mm/s by the motorised stage, however, this could be increased to provide faster imaging rates by using a faster translation stage. The velocity of the motor could be increased by a factor of 4 to 20 mm/s, whilst still maintaining an A-line separation below the recorded lateral resolution limit without changing the current A-line acquisition rate (200 Hz). This would result in an image acquisition time of 1 s for the same image aperture size used here. Additionally, the A-line repetition rate could be increased to allow for smaller A-line separations at faster pull-back velocities. Crucially, no image reconstruction was needed to provide high-resolution images. Image processing only used simple filtering and concatenation of consecutive A-lines to form the image. This is well-suited to *in vivo* applications where small positioning errors make image reconstruction unreliable [29].

The measured image resolution found using a tungsten wire phantom was *ca.* 100 µm and 200 µm as measured in the depth (axial) and $x$ (lateral) axes, respectively (Fig. 4(a), (b)). These are comparable to commonly used clinical intravascular ultrasound transducers [36,37] and previously reported OpUS transducers [26,30]. The tungsten wires appeared in the image as tilted ellipses (Fig. 4(a)) due to the finite separation between the transmit and receive elements of the transducer. Thus, the distance from the transmitter and receiver to the target, respectively, was different for the same lateral offset from the target on either side of the target. The resolution as measured along the tilted axis will likely be larger than the measured lateral resolution, due to the increased spreading of the point-spread-function. The high degree of beam collimation was supported by the constant lateral resolution with increasing depth. This is valuable for imaging in a clinical context, where deeper structures may be of interest to the operator. Despite the excellent resolution values, they might be improved in future work. The axial resolution could be improved by extending the bandwidth of the plano-concave microresonator. This can be achieved by reducing the cavity length, but would come at the expense of sensitivity.

Biomedical Optics EXPRESS

Alternatively, the generated ultrasound bandwidth could be increased by reducing the thickness of the ultrasound generating coating, as has been highlighted in previous studies [7]. The lateral resolution was dependent on the beamwidth since no image reconstruction was employed. The narrow beamwidth generated in this work (*ca.* 0.5 mm at a depth of 1.5 mm) resulted from a combination of the generated acoustic bandwidth and the relatively large ultrasound generator aperture. The aperture size was defined by the excitation light spot size, which resulted primarily from guided laser light within the capillary reflecting from the polished 45° surface, giving an aperture size of *ca.* $0.55 \times 0.55$ mm. This could be improved by using a concave ultrasound generating surface to achieve a tighter focus. Further, this reduction in beam divergence would be expected to improve the signal-to-noise ratio for a given depth and thus lead to an improvement in the achievable imaging depth.

The acquired porcine aorta image demonstrated clinically relevant details with both the vessel surface and subsurface structure providing differing contrast. The tilting of the point-spread-functions observed from the tungsten wire phantom did not appear to adversely affect the vessel definition in the aorta image. The full thickness of the aorta (*ca.* 1.5 mm) was imaged and a signal-to-noise ratio of 27 dB was achieved without the use of averaging or image reconstruction. Further, the side branch in the aorta was clearly visualised as a region with no signal, demonstrating the ability of the device to resolve relevant features. The signal-to-noise and imaging depth might be improved in future studies by increasing the generated ultrasound pressure and beam collimation as already highlighted.

The study presented here represents a radical step in the design of ultrasound transducers. The novel approach using a dual-clad optical fibre, allowing for the delivery of both multimode and single mode light for ultrasound generation and reception, respectively, allowed for the fabrication of an OpUS transducer capable of high resolution tissue imaging with a very small form factor. This work opens the pathway to preclinical *in vivo* imaging with such a device. To enable this in future work, the transducer will be built into a catheter designed for use *in vivo*, within vessels and ducts. Further, the 2D linear imaging presented here could be extended to include rotational imaging, like that previously presented using two optical fibres [27]. This would require the integration of a rotary junction into the console to enable rotation of the transducer without twisting the optical fibre. It is expected that this breakthrough in OpUS transducer fabrication will lead to new minimally invasive imaging applications and devices.

**Funding.** Royal Academy of Engineering (RF/201819/18/125); Wellcome Trust (203145/Z/16/Z); European Research Council (74119).

**Disclosures.** RJC & AED own shares in Echopoint Medical Ltd. PCB & EZZ own shares in DeepColor SAS.

**Data availability.** Data underlying the results presented in this paper are not publicly available at this time but may be obtained from the authors upon reasonable request.

## References

1. M. Alkhouli, Z. M. Hijazi, D. R. Holmes, C. S. Rihal, and S. E. Wiegers, "Intracardiac echocardiography in structural heart disease interventions," JACC: Cardiovasc. Interv. **11**(21), 2133–2147 (2018).
2. S. Sonoda, K. Hibi, H. Okura, K. Fujii, Y. Honda, and Y. Kobayashi, "Current clinical use of intravascular ultrasound imaging to guide percutaneous coronary interventions," Cardiovasc. Interv. Ther. **35**(1), 30–36 (2020).
3. J. Wang, Z. Zheng, J. Chan, and J. T. W. Yeow, "Capacitive micromachined ultrasound transducers for intravascular ultrasound imaging," Microsyst. Nanoeng. **6**(1), 73 (2020).
4. M. J. Gounis, G. J. Ughi, M. Marosfoi, D. K. Lopes, D. Fiorella, H. G. Bezerra, C. W. Liang, and A. S. Puri, "Intravascular optical coherence tomography for neurointerventional surgery," Stroke **50**(1), 218–223 (2019).
5. A. Boi, A. D. Jamthikar, L. Saba, D. Gupta, A. Sharma, B. Loi, J. R. Laird, N. N. Khanna, and J. S. Suri, "A survey on coronary atherosclerotic plaque tissue characterization in intravascular optical coherence tomography," Curr. Atheroscler. Rep. **20**(7), 33 (2018).
6. B. T. Cox and P. C. Beard, "Fast calculation of pulsed photoacoustic fields in fluids using k -space methods," J. Acoust. Soc. Am. **117**(6), 3616–3627 (2005).
7. S. Noimark, R. J. Colchester, B. J. Blackburn, E. Z. Zhang, E. J. Alles, S. Ourselin, P. C. Beard, I. Papakonstantinou, I. P. Parkin, and A. E. Desjardins, "Carbon-nanotube-PDMS composite coatings on optical fibers for all-optical ultrasound imaging," Adv. Funct. Mater. **26**(46), 8390–8396 (2016).

Biomedical Optics EXPRESS


8. S. Noimark, R. J. Colchester, R. K. Poduval, E. Maneas, E. J. Alles, T. Zhao, E. Z. Zhang, M. Ashworth, E. Tsolaki, A. H. Chester, N. Latif, S. Bertazzo, A. L. David, S. Ourselin, P. C. Beard, I. P. Parkin, I. Papakonstantinou, and A. E. Desjardins, "Polydimethylsiloxane composites for optical ultrasound generation and multimodality imaging," Adv. Funct. Mater. **28**(9), 1704919 (2018).
9. R. J. Colchester, E. J. Alles, and A. E. Desjardins, "A directional fibre optic ultrasound transmitter based on a reduced graphene oxide and polydimethylsiloxane composite," Appl. Phys. Lett. **114**(11), 113505 (2019).
10. S. Bodian, R. J. Colchester, T. J. Macdonald, F. Ambroz, M. Briceno de Gutierrez, S. J. Mathews, Y. M. M. Fong, E. Maneas, K. A. Welsby, R. J. Gordon, P. Collier, E. Z. Zhang, P. C. Beard, I. P. Parkin, A. E. Desjardins, and S. Noimark, "CuInS 2 quantum dot and polydimethylsiloxane nanocomposites for all-optical ultrasound and photoacoustic imaging," Adv. Mater. Interfaces **8**(20), 2100518 (2021).
11. R. J. Colchester, C. D. Little, E. J. Alles, and A. E. Desjardins, "Flexible and directional fibre optic ultrasound transmitters using photostable dyes," OSA Continuum **4**(9), 2488–2495 (2021).
12. S. H. Lee, Y. Lee, and J. J. Yoh, "Reduced graphene oxide coated polydimethylsiloxane film as an optoacoustic transmitter for high pressure and high frequency ultrasound generation," Appl. Phys. Lett. **106**(8), 081911 (2015).
13. Y. Hou, J.-S. Kim, S. Ashkenazi, S.-W. Huang, L. J. Guo, and M. O'Donnell, "Broadband all-optical ultrasound transducers," Appl. Phys. Lett. **91**(7), 073507 (2007).
14. W.-Y. Chang, W. Huang, J. Kim, S. Li, and X. Jiang, "Candle soot nanoparticles-polydimethylsiloxane composites for laser ultrasound transducers," Appl. Phys. Lett. **107**(16), 161903 (2015).
15. P. Oser, J. Jehn, M. Kaiser, O. Düttmann, F. Schmid, L. Schulte-Spechtel, S. S. Rivas, C. Eulenkamp, C. Schindler, C. U. Grosse, and D. Wu, "Fiber-optic photoacoustic generator realized by inkjet-printing of cnt-pdms composites on fiber end faces," Macromol. Mater. Eng. **306**(2), 2000563 (2021).
16. T. Zhao, L. Su, and W. Xia, "Optical ultrasound generation and detection for intravascular imaging: a review," J. Healthc. Eng. **2018**, 1–14 (2018).
17. G. Wissmeyer, M. A. Pleitez, A. Rosenthal, and V. Ntziachristos, "Looking at sound: optoacoustics with all-optical ultrasound detection," Light: Sci. Appl. **7**(1), 53 (2018).
18. B.-Y. Hsieh, S.-L. Chen, T. Ling, L. J. Guo, and P.-C. Li, "All-optical scanhead for ultrasound and photoacoustic imaging—Imaging mode switching by dichroic filtering," Photoacoustics **2**(1), 39–46 (2014).
19. T. Ling, S.-L. Chen, and L. J. Guo, "High-sensitivity and wide-directivity ultrasound detection using high Q polymer microring resonators," Appl. Phys. Lett. **98**(20), 204103 (2011).
20. A. Rosenthal, D. Razansky, and V. Ntziachristos, "High-sensitivity compact ultrasonic detector based on a pi-phase-shifted fiber bragg grating," Opt. Lett. **36**(10), 1833–1835 (2011).
21. Y. Hazan and A. Rosenthal, "Simultaneous multi-channel ultrasound detection via phase modulated pulse interferometry," Opt. Express **27**(20), 28844–28854 (2019).
22. E. Z. Zhang and P. C. Beard, "A miniature all-optical photoacoustic imaging probe," in *Proceedings of SPIE, Photons Plus Ultrasound*, vol. 7899 A. A. Oraevsky and L. V. Wang, eds. (2011), pp. 78991F–1–78991F–6.
23. E. Z. Zhang and P. C. Beard, "Characteristics of optimized fibre-optic ultrasound receivers for minimally invasive photoacoustic detection," in *Proc. of SPIE, Photons Plus Ultrasound: Imaging and Sensing*, vol. 9323 A. A. Oraevsky and L. V. Wang, eds. (2015), pp. 932311–1–9.
24. J. A. Guggenheim, J. Li, T. J. Allen, R. J. Colchester, S. Noimark, O. Ogunlade, I. P. Parkin, I. Papakonstantinou, A. E. Desjardins, E. Z. Zhang, and P. C. Beard, "Ultrasensitive plano-concave optical microresonators for ultrasound sensing," Nat. Photonics **11**(11), 714–719 (2017).
25. O. Ülgen, R. Shnaiderman, C. Zakian, and V. Ntziachristos, "Interferometric optical fiber sensor for optoacoustic endomicroscopy," J. Biophotonics **14**, e202000501 (2021).
26. R. J. Colchester, E. Z. Zhang, C. A. Mosse, P. C. Beard, I. Papakonstantinou, and A. E. Desjardins, "Broadband miniature optical ultrasound probe for high resolution vascular tissue imaging," Biomed. Opt. Express **6**(4), 1502–1511 (2015).
27. R. J. Colchester, C. Little, G. Dwyer, S. Noimark, E. J. Alles, E. Z. Zhang, C. D. Loder, I. P. Parkin, I. Papakonstantinou, P. C. Beard, M. C. Finlay, R. D. Rakhit, and A. E. Desjardins, "All-Optical Rotational Ultrasound Imaging," Sci. Rep. **9**(1), 5576 (2019).
28. M. C. Finlay, C. A. Mosse, R. J. Colchester, S. Noimark, E. Z. Zhang, S. Ourselin, P. C. Beard, R. J. Schilling, I. P. Parkin, I. Papakonstantinou, and A. E. Desjardins, "Through-needle all-optical ultrasound imaging in vivo: a preclinical swine study," Light: Sci. Appl. **6**(12), e17103 (2017).
29. E. J. Alles, S. Noimark, E. Zhang, P. C. Beard, and A. E. Desjardins, "Pencil beam all-optical ultrasound imaging," Biomed. Opt. Express **7**(9), 3696–3704 (2016).
30. G. Li, Z. Guo, and S.-L. Chen, "Miniature all-optical probe for large synthetic aperture photoacoustic-ultrasound imaging," Opt. Express **25**(21), 25023–25035 (2017).
31. R. J. Colchester, J. T. Moore, T. M. Peters, M. C. Finlay, and A. E. Desjardins, "Real-time all-optical ultrasound imaging of a dynamic heart valve phantom," in *Frontiers in Biophotonics and Imaging*, vol. 11879 S. Mahajan and S. Reichelt, eds., International Society for Optics and Photonics (SPIE, 2021), pp. 32–37.
32. X. Guo, N. Wu, J. Zhou, C. Du, and X. Wang, "Validation of an ultrasound transducer's generation and receiving function on one single-mode fiber," Opt. Lasers Eng. **127**, 105962 (2020).

Biomedical Optics EXPRESS


33. X. Wen, B. Zhang, W. Wang, F. Ye, S. Yue, H. Guo, G. Gao, Y. Zhao, Q. Fang, C. Nguyen, X. Zhang, J. Bao, J. T. Robinson, P. M. Ajayan, and J. Lou, "3D-printed silica with nanoscale resolution," Nat. Mater. **20**(11), 1506–1511 (2021).
34. H. Zhang, L. Huang, M. Tan, S. Zhao, H. Liu, Z. Lu, J. Li, and Z. Liang, "Overview of 3d-printed silica glass," Micromachines **13**(1), 81 (2022).
35. J. Li, P. Fejes, D. Lorenser, B. C. Quirk, P. B. Noble, R. W. Kirk, A. Orth, F. M. Wood, B. C. Gibson, D. D. Sampson, and R. A. McLaughlin, "Two-photon polymerisation 3D printed freeform micro-optics for optical coherence tomography fibre probes," Sci. Rep. **8**(1), 14789 (2018).
36. M. R. Elliott and A. J. Thrush, "Measurement of resolution in intravascular ultrasound images," Physiol. Meas. **17**(4), 259–265 (1996).
37. M. Ono, H. Kawashima, H. Hara, C. Gao, R. Wang, N. Kogame, K. Takahashi, P. Chichareon, R. Modolo, M. Tomaniak, J. J. Wykrzykowska, J. J. Piek, I. Mori, B. K. Courtney, W. Wijns, F. Sharif, C. Bourantas, Y. Onuma, and P. W. Serruys, "Advances in ivus/oct and future clinical perspective of novel hybrid catheter system in coronary imaging," Front. Cardiovasc. Med. **7**, 119 (2020).